RSC Advances

ROYAL SOCIETY OF CHEMISTRY

www.rsc.org/advances

Journal Name

ARTICLE

Novel yet simple strategy to fabricate visible light responsive C,N-TiO_2/g-C_3N_4 heterostructures with significantly enhanced photocatalytic hydrogen generation

Received 00th January 20xx,
Accepted 00th January 20xx

DOI: 10.1039/x0xx00000x

www.rsc.org/

Wei Chen[a], Tian-Yu Liu[a], Ting Huang[a], Xiao-Heng Liu[a,*],Guo-Rong Duan[a], Xu-Jie Yang[a] and Shen-Ming Chen[b,*]

In this report, we first successfully designed and fabricated the novel C,N co-doped titanium dioxide nanoparticles/graphite-like carbon nitrogen ultrathin nanosheets (C,N-TiO_2 NPs/g-C_3N_4) heterostructures, wherein the C,N-TiO_2 NPs were in-site growth on the porous g-C_3N_4 ultrathin nanosheets (NSs) by a simple one-pot solvothermal route with the assistance of concentrated nitric acid. The resulting C,N-TiO_2 NPs/g-C_3N_4 nanocomposite photocatalysts were systematically characterized by powder X-ray diffraction (PXRD), Fourier transform infrared spectroscopy (FT-IR), diffuse reflectance spectroscopy (DRS), transmission electron microscopy (TEM), X-ray photoelectron spectroscopy (XPS), photoluminescence (PL) spectroscopy, transient photocurrent-time (I-t) curves and electrochemical impedance spectroscopy (EIS) Nyquist plots. The photocatalytic ability was evaluated by photocatalytic water splitting for hydrogen evolution. These studies indicate that C,N-TiO_2 NPs/g-C_3N_4 composites exhibit superior ability for hydrogen generation than single C,N-TiO_2 NPs and pure g-C_3N_4 NSs under visible light illumination. The optimal composites with 3 wt% C,N-TiO_2 NPs/g-C_3N_4 showed a highest hydrogen evolution rate of 39.18 $\mu mol \cdot g^{-1} \cdot h^{-1}$, which is about 10.9 and 21.3 times than those of C,N-TiO_2 NPs and pure g-C_3N_4 NSs, respectively. The improved visible photocatalytic H_2 evolution can be attributed to improved optical absorption and the lengthening lifetime of charge carriers' pairs as results of the C,N elmental codoping and the construction of intimate heterogeneous interface. This simple and feasible method for the fabrication of highly-efficient visible light responsive catalysts provide a great applied potential in energy generation.

1. Introduction

With the rapidly increasing amount of population and highly rate development of industrialization, recent years have witnessed hugely serious energy crisis and the environmental contamination resulted from the depletion of fossil fuel and the emission of poisonous and harmful substances. These challenges force us to develop new energies to replace the traditional energies. Hydrogen energy, widely popular approval as a clean energy, is a promising choice to resolve the above-mentioned bottlenecks since the Fujishima and Honda reported the photoelectrochemical hydrogen evolution by using the TiO_2 electrode in 1972.[1] However, because of the relatively wide band gap with value of about 3.2 eV for the anatase phase and 3.0 eV for the rutile phase, the pure TiO_2 just exhibits ultraviolet light response to generate holes and electrons pairs, which are important active species responsible for photocatalytic process. Unluckily, the ultraviolet light only makes up 4% of the total solar spectrum reaching the surface of the earth. The limited UV-driven activity largely inhibits the practical application of pure TiO_2. Besides, the speedy recombination of photogenerated holes and electrons pairs is another fatal flaw, leading to low quantum efficiency of original TiO_2. Therefore, huge efforts have been devoted to extending the spectrum absorption into visible light region and lengthening the lifespan of charge carrier pairs by means of noble metal loading,[2-4] elemental doping [5-7] or co-doping [8,9] and heterogeneous coupling [10-12].

So now many practices with different fabrication routes have proven that elemental doping, such as C, N, S, F, Ti doping or co-doping, is a feasible strategy to modify the photocatalytic activity of TiO_2 materials, which would not only narrow the band gap of TiO_2 to increase the light absorption but also introduce more active sites to lengthen the lifetime of photogenerated holes and electrons pairs.[13-15] To further optimize the photocatalytic activity, on the basis of original TiO_2 or doped TiO_2, researchers have constructed the heterogeneous composites by coupling with other materials.[16] Graphitic carbon nitrogen (g-C_3N_4), with the features of appropriate band gap, abundant available, simple preparation and highly stability at different environments, were widely composited with TiO_2 and modified TiO_2. Recently, Wang et al. [17] reported the fabrication of TiO_2/g-C_3N_4 by calcination route and their highly-efficient photocatalytic activity for hydrogen generation from water

[a] Key Laboratory of Education Ministry for Soft Chemistry and Functional Materials, Nanjing University of Science and Technology, Nanjing 210094, China
[b] Electroanalysis and Bioelectrochemistry Lab, Department of Chemical Engineering and Biotechnology, National Taipei University of Technology, No.1, Section 3, Chung-Hsiao East Road, Taipei 106, Taiwan (ROC).
E-mail: xhliu@mail.njust.edu.cn(X.H. Liu); smchen78@ms15.hinet.net(S.M. Chen;)
Electronic Supplementary Information (ESI) available: [details of any supplementary information available should be included here]. See DOI: 10.1039/x0xx00000x

splitting. Li et al. [18] utilized the similar synthetic strategy to prepare the Ti^{3+} self-doped TiO_2/g-C_3N_4 heterojunctions, which shows significantly enhanced photocatalytic performance under LED light irradiation. Also, Zhou et al. [19] reported obvious photocatalytic enhancement of hybrid TiO_2/g-C_3N_4 via ball milling method. Obviously, although the enhancement of photocatalytic activity has been realized as results of the construction of heterogeneous junctions by coupling between TiO_2 (modified TiO_2) and g-C_3N_4, the deficiency of these researches focuses on the composite with bulk g-C_3N_4, which often exhibits high recombination rate of photo-generated charge carriers due to the formation of a vast grain boundary defects during the thermal polycondensation and the low specific surface area.[20] Han et al.[21] in situ prepared the N-TiO_2/g-C_3N_4 nanosheets heterostructures by a simple electrospinning process combined with a modified heat-etching method, which present highly efficient degradation activity and photocatalytic H_2 production with the exposure of simulated solar light.

To our knowledge, there is no report involving the synthesis of C,N-TiO_2 NPs/g-C_3N_4 ultrathin nanosheets heterostructures until now. Herein, we demonstrate the simple and novel strategy to prepare the C,N-TiO_2 NPs/g-C_3N_4 NSs nanocomposites with highly efficient catalytic performance for hydrogen generation. The fabrication strategy of C,N-TiO_2 NPs/g-C_3N_4 is simple and exclusive of calcination treatment at high temperature condition. Different from the previous reports of C-TiO_2 and N-TiO_2,[5,7] here the anion group (-C_4H_9O) in tetrabutyl titanate (TBT) serve as carbon doping agent and the addition of concentrated HNO_3 is used as inhibitor to control the rate of hydrolysis of TBT and employed as the source of N doping reagent.

2. Experimental

2.1 Preparation

Melamine ($C_6H_6N_6$), tetrabutyl titanate ($C_{16}H_{36}O_4Ti$), absolute ethanol (C_2H_6O) and concentrated nitric acid (HNO_3) are provided by Sinopharm Chemical Reagent Co., Ltd. (Shanghai, China). All reagents were used without further purification. Porous g-C_3N_4 ultrathin nanosheets were prepared according to our reported procedure.[22] The specific surface area of g-C_3N_4 nanosheets was calculated to be 198.5 $m^2 \cdot g^{-1}$, with a nearly 9-fold enhancement in that of bulk g-C_3N_4 (22.3 $m^2 \cdot g^{-1}$). C,N-TiO_2 NPs /g-C_3N_4 samples were fabricated by a simple solvothermal route with the presence of concentrated nitric acid. During the preparation process, a desired amount of TBT was dissolved in 30 mL of absolute ethanol containing 1 mL of concentrated HNO_3 and 200 mg of porous g-C_3N_4 NSs. After 6h stirring, the mixed solution was transferred to a 40 mL Teflon-lined stainless steel autoclave with up to 75% of the total volume. The auto-clave was sealed and kept at 453 K for 24 h. For comparison, the C,N-TiO_2 NPs was also synthesized at same condition without addition of porous g-C_3N_4 NSs.

2.2 Characterization

Powder X-ray diffraction (PXRD) patterns were recorded on a Bruker Advanced D8 diffractometer (Germany) at 40 kV and 40 mA with monochromatic high intensity Cu Kα radiation (λ=0.15418 nm). Sample morphology and microstructure were observed by a transmission electron microscope (TEM) (JEOL JEM-2100) and high resolution transmission electron microscope (HRTEM) at 200 kV accelerating voltage. Fourier transform infrared (FT-IR) spectra were measured by a Nicolet IS10 infrared spectrometer. The optical properties of the samples were measured using UV-vis diffuse reflectance spectroscopy (Shimadzu UV-2500) with $BaSO_4$ as the reflectance standard. The surface composition analysis and electronic binding energy of samples were acquired by a Thermo ESCALAB 250Xi X-ray photoelectron spectrometer under an Al Kα radiation (hv = 1486.6 eV). Solid-state fluorescence measurements (λ_{ex} = 325 nm) were recorded from 350 to 700 nm on a JASCO FP-6500 type fluorescence spectrophotometer using 1 nm slit width. Raman spectra (RS) were recorded by a Renishaw Invia Raman Microscope using argon ion laser from 100 to 2000 cm^{-1}. The photoelectrochemical properties were measured on a CHI-660E electrochemical workstation (Shanghai Chenhua Instrument Co., Ltd, China) in a standard three-electrode system using the prepared samples with an active area of ca. 0.5 cm×0.5 cm as the working electrodes, a platinum wire as the counter electrode, and Ag/AgCl as the reference electrode and Na_2SO_4 (0.1 M) aqueous solution was used as the electrolyte. Electrochemical impedance spectra (EIS) were recorded at the open circuit potential by applying an AC voltage with 5 mV amplitude in the frequency range from 0.01 Hz to 100 kHz.

2.3 Photocatalytic tests

The photocatalytic hydrogen evolution from water splitting was detected using the PES-10A evaluation system. Typically, 100 mg of photocatalyst was dispersed in 100 mL of aqueous solution containing 10 vol% triethanolamine (TEOA) acted as sacrificial electron donors. Before the photocatalytic reaction, the system was evacuated and refilled with argon gas several times to remove the air inside the reaction system. This process was conducted until the residual air content checked by an online gas chromatography (GC-1690, Hangzhou JieDao Tech Co., Ltd, China) was negligible. Then, the reactor was irradiated from the side using a 300 W xenon lamp equipped with an optical cut-off filter to remove ultraviolet illumination (λ > 400 nm). The reaction was carried out for 8 h, and the produced hydrogen gas was analyzed by GC-1690 using an online sampling loop (3.5 mL) at intervals of 1 h. The GC 1690 system was equipped with a thermal conductivity detector. Reference experiments were performed without photocatalyst in the presence of light and with photocatalyst in the dark. In both cases, no production of hydrogen was observed.

3. Results and discussion

The crystallographic structure and phase purity of C,N-TiO_2 NPs/g-C_3N_4 nanocomposites were determined by X-ray diffraction technique as displayed in Fig.1a In the case of pure g-C_3N_4 NSs, two obvious diffraction peaks with 2θ value of 13.2 ^{o} and 27.8 ^{o} belong to the (100) and (002) diffraction planes of g-C_3N_4 NSs. The strong (002) peak represents inter-layer stacking of conjugated aromatic system, whereas weak one of (100) plane arises from the in-plane structural packing motif of tri-s-triazine units, respectively.[23,24] The

XRD pattern of C,N-TiO_2 NPs are in well agreement with anatase structure (JCPDS No. 21-1272). The characteristic diffraction peaks of (101) plane of C,N-TiO_2 NPs and all diffraction peaks ascribed to g-C_3N_4 NSs are presented in C,N-TiO_2 NPs/g-C_3N_4 composites, suggesting the coexistence of C,N-TiO_2 NPs and g-C_3N_4 NSs in C,N-TiO_2 NPs/g-C_3N_4 composites. No impurity phases are detected, indicative of high purity of as-prepared catalysts.

The FT-IR spectra of pure g-C_3N_4 NSs and a series of C,N-TiO_2 NPs/g-C_3N_4 composites are displayed in Fig.1b. For pristine g-C_3N_4 NSs, a wide absorption band between 3000 cm^{-1} and 3600 cm^{-1} corresponds to stretching vibration of O–H of the absorbed water molecule and N–H stretching vibration modes of residual NH_2 attached to the sp^2 hybridized carbon or NH groups at the defect sites of the aromatic ring.[25] While several strong characteristic peaks located between 1200 cm^{-1} and 1700 cm^{-1} are explained as typical stretching vibration of CN heterocycles.[26] Additionally, a sharp peak at 808 cm^{-1} is assigned to breathing mode of triazine units.[27] The FT-IR spectra of C,N-TiO_2 NPs/g-C_3N_4 composites exhibit the overlap of the spectra of both C,N-TiO_2 NPs (Fig. S2) and g-C_3N_4 NSs, which suggests the coexistence of C,N-TiO_2 NPs and g-C_3N_4 NSs in composite samples. These results are in well accordance with XRD analysis.

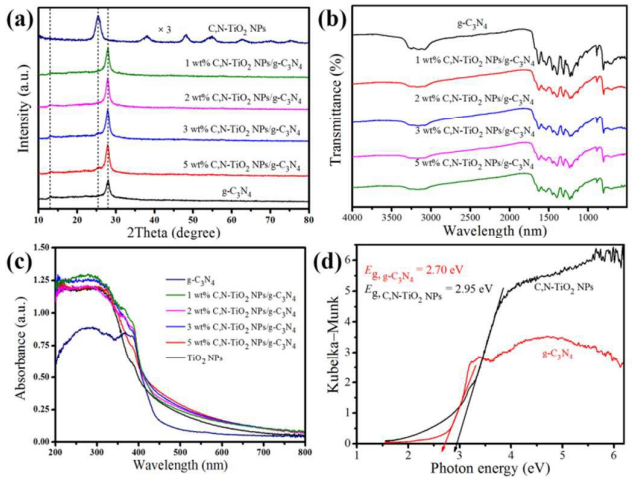

Fig.1 (a) Typical XRD pattern, (b) FT-IR spectra, (c) UV-vis diffuse reflectance spectra and (d) corresponding to Kubelka-Munk transformed function of different photocatalysts.

The optical properties of as-prepared C,N-TiO_2 NPs, pure g-C_3N_4 NSs as well as C,N-TiO_2 NPs/g-C_3N_4 composites were detected by UV-vis diffuse reflectance spectra (DRS) and the corresponding band gap energies were estimated by Kubelka-Munk equation. Fig.1c shows the DRS spectra of the hybrid C,N-TiO_2 NPs/g-C_3N_4 photocatalysts, from which, we can clearly found that g-C_3N_4 exhibits typical light absorption in the region ranging from 200 nm to 450nm, which is ascribed to the charge transfer response of g-C_3N_4 NSs from the valence band formed with N 2p orbits to the conduction band populated by C 2p orbits. [28] Interestingly, the C,N-TiO_2 NPs is able to absorb visible light with the maximum wavelength up to 460 nm as a result of the doping level generated by C and N atom co-doping. Compared with that of single component, all the C,N-TiO_2 NPs/g-C_3N_4 samples exhibit significantly improved light-harvesting capability. Such red shifts of light absorption might be attributed to the beneficial interaction between C,N-TiO_2 NPs and g-C_3N_4 NSs resulted from the construction of close heterojunction interface. The band gap energies (Fig.1d) of C,N-TiO_2 NPs and pure g-C_3N_4 NSs calculated by Kubelka-Munk formula are 2.95 eV and 2.70 eV, respectively.

The sample morphology and microstructure information were investigated by TEM and HRTEM, as shown in Fig.2. As expected, the C,N-TiO_2 NPs with the diameter of several nanometers were homogeneously immobilized on the surface of ultrathin g-C_3N_4 NSs by one-pot solvothermal route, which is favorable to the formation of intimate heterogeneous interface. The size of C,N-TiO_2 NPs in C,N-TiO_2 NPs/g-C_3N_4 heterojunction photocatalysts is similar to that of pristine C,N-TiO_2 NPs and no agglomeration structures of C,N-TiO_2 NPs located on the surface of g-C_3N_4 NSs have be observed. This good dispersion is benefit to the separation of photo-induced holes and electrons pairs and thus is responsible for the enhancement of photocatalytic performance. From the high-resolution image of C,N-TiO_2 NPs/g-C_3N_4 composites, the sharp-edged lattice images ascribed to C,N-TiO_2 NPs are presented with the lattice spacing of 0.352 nm, corresponding to (101) crystallographic planes of anatase TiO_2.

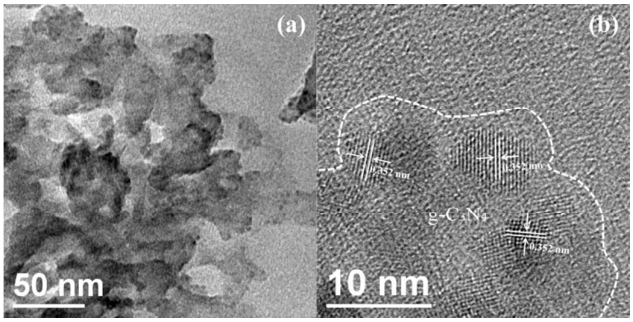

Fig.2 (a) TEM image and (b) HR-TEM image of 3wt% C,N-TiO_2 NPs/g-C_3N_4 nanocomposites.

To verify the elemental categories and chemical status in C,N-TiO_2 NPs/g-C_3N_4 composites, the X-ray photoelectron spectra (XPS) of C,N-TiO_2 NPs, g-C_3N_4 NSs as well as C,N-TiO_2 NPs/g-C_3N_4 composites were measured. Fig.3a displays the XPS survey of these three samples. It is obvious that C,N-TiO_2 NPs/g-C_3N_4 composites is composed of C, N, Ti and O elements, which well confirms the coexistence of C,N-TiO_2 NPs and g-C_3N_4 NSs in C,N-TiO_2 NPs/g-C_3N_4 hybrid sample. The typical high resolution XPS spectra of C 1s, N 1s and Ti 2p in different samples are also shown in Fig. 3(b-d). The C 1s high-resolution spectrum displays two peaks centering at 284.8, and 288.0 eV for pure g-C_3N_4 NSs, 284.8 and 287.9 eV for composite sample, which can be attributed to the contaminated carbon and the sp^2-bonded carbon (-N=C-N) in graphitic carbon nitride, respectively.[29] The C 1s peak, originating from the sp^2 carbon, shifts to a lower binding energy direction after coupling with C,N-TiO_2 NPs, indicating the variation of chemical environment of sp^2 carbon via chemical bonds. While the N 1s spectrum of g-C_3N_4 NSs can be deconvoluted into four different Gaussian-Lorenzian peaks centered at the binding energies of 398.3, 398.9, 400.5 and 404.2 eV. The main peak at 398.3 eV could be ascribed to nitrogen atoms

sp^2-hybridized to carbon atom (C=N-C). [30] The characteristic peak at 398.9 eV is related to either N-$(C)_3$ groups linking structural motif (C_6N_7) or amino groups ($(C)_2$–N–H) connecting with structural defects and incomplete condensation. [25,31] The weak peak with the binding energy of 400.5 eV is resulted from N bonded to three carbon atoms to develop the N–$(C)_3$ group in the aromatic cycles. [32] However, due to the coupling with C,N-TiO_2 NPs, the peaks belonging to N 1s at 398.9 and 400.5 eV separately shift to 399.0 and 400.7 eV, which means the presence of interaction between C,N-TiO_2 NPs and g-C_3N_4 NSs. We attribute this interaction to the generation of C-N-Ti bonds as evidence provided by high-resolution XPS spectra of Ti 2p region. The binding energies of Ti 2p3/2 and Ti 2p1/2 are located at 458.5 and 464.2 eV, which are very close with values of Ti^{4+} in N-TiO_2. [33] The obvious shifts of Ti 2p peaks in hybrid sample with respect to that of Ti^{4+} in C,N-TiO_2 NPs further confirm the existence of C-N-Ti bonds at the interface of C,N-TiO_2 NPs and g-C_3N_4 NSs.

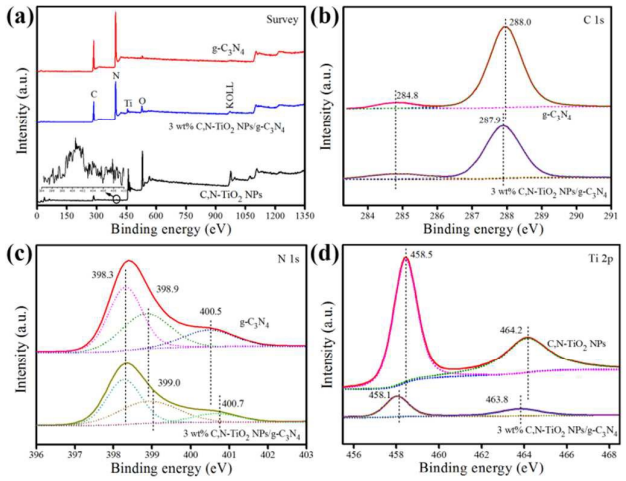

Fig.3 XPS spectra of original C,N-TiO_2 NPs, pure g-C_3N_4 and 3 wt% C,N-TiO_2 NPs/g-C_3N_4: (a) survey spectra, (b) C 1s ,(c) N 1s and (d) Ti 2p region.

The photocatalytic activities of those C,N-TiO_2 NPs/g-C_3N_4 composites were investigated by hydrogen production from water splitting with the addition of 10 vol% TEOA as sacrificial reagent under the visible light irradiation. Controllable experiments suggested that no appreciable H_2 produced in the absence of either photocatalyst or light irradiation. Fig.4 displays the H_2 generation curves (Fig.4a) and the average rate of H_2 evolution (Fig.4b) over C,N-TiO_2 NPs/g-C_3N_4 hybrid samples with different concentration of C,N-TiO_2 NPs loadings. As shown in Fig.4a, the total amount of H_2 evolution during the 8 h photoredox reaction increases upon enhancing the C,N-TiO_2 NPs contents from 0 to 3 wt % and then decreases with further enhancement to 5 wt %. Obviously, the pure C,N-TiO_2 NPs and g-C_3N_4 NSs alone show negligible photocatalytic performance for H_2 production with average value of 3.59 $\mu mol \cdot g^{-1} \cdot h^{-1}$ and 1.84 $\mu mol \cdot g^{-1} \cdot h^{-1}$, respectively. The extremely low photocatalytic activity of g-C_3N_4 NSs possibly originates from some vast grain boundary defects formed during the high temperature preparation process, which hugely promote the faster recombination of photo-induced holes and electrons pairs.[19]

However, after assembly of C,N-TiO_2 NPs onto the g-C_3N_4 NSs, the obtained C,N-TiO_2 NPs/g-C_3N_4 nanocomposites can response broader visible light region and form more photo-induced holes and electrons, thus benefiting the photocatalytic activities for H_2 evolution. In this hybrid system, the optimal content of C,N-TiO_2 NPs immobilized on the g-C_3N_4 NSs to achieve the highest photocatalytic water splitting is determined to 3 wt%. The average H_2 evolved rate over 3 wt% C,N-TiO_2 NPs/g-C_3N_4 is 39.18 $\mu mol \cdot g^{-1} \cdot h^{-1}$, which is ca. 10.9 times higher than that of sole C,N-TiO_2 NPs and 21.3 times higher than that of pure g-C_3N_4 NSs.

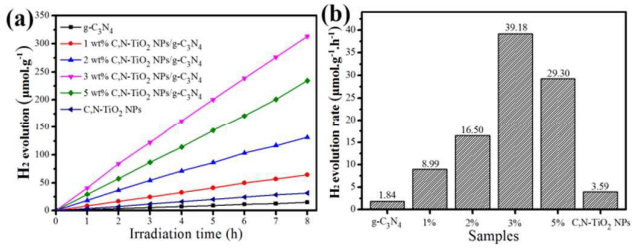

Fig.4 (a) Hydrogen evolution and (b) corresponding to hydrogen production rate from water splitting by different samples under visible light irradiation.

The important factors for 3 wt% C,N-TiO_2 NPs/g-C_3N_4 nanocomposites with the highest photocatalytic activity lie in the synergistic effect of element doping of C and N into TiO_2 and the construction of intimate heterojunction structure between C,N-TiO_2 NPs and g-C_3N_4 NSs, namely, the enhancement of light absorption and the lengthen of charge carrier lifetime. The C,N-TiO_2 NPs in hybrid system could remarkably strengthen the light absorption to extend into visible light region, from which, the doped TiO_2 NPs here was similar with the role cocatalyst played. Moreover, due to the construction of intimate heterojunction interface and well-matched band edge, the C,N-TiO_2 NPs also could act as electron acceptors and transfer channels, thus improving the charge separation efficiency. As can be seen in Fig. 5, upon photo-irradiation, C,N-TiO_2 NPs and g-C_3N_4 could easily absorb visible light to generate hole-electron pairs. According to previous reports, the conduction band (CB) and valence band (VB) potential could be determined to be −1.12 and +1.58 eV for g-C_3N_4, -0.29 and 2.91 eV for pristine TiO_2.[18,22] Therefore, the photo-generated electrons in conduction band (CB) of the g-C_3N_4 would directly inject into that of C,N-TiO_2 NPs, meanwhile the holes could migrate from C,N-TiO_2 NPs to VB of g-C_3N_4. However, the electrons accumulated in the CB of C,N-TiO_2 NPs would be extracted by oxygen vacancy originated from elemental doping.[34] Such electron transfer paths effectively suppress their recombination thus benefiting the photocatalytic activity.

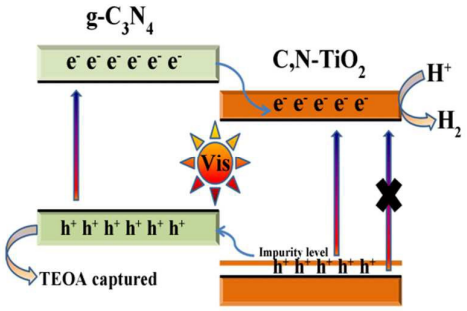

Fig. 5 Schematic illustration of charge transfer and separation in C,N-TiO_2 NPs/g-C_3N_4 photocatalysts for hydrogen production under visible light irradiation.

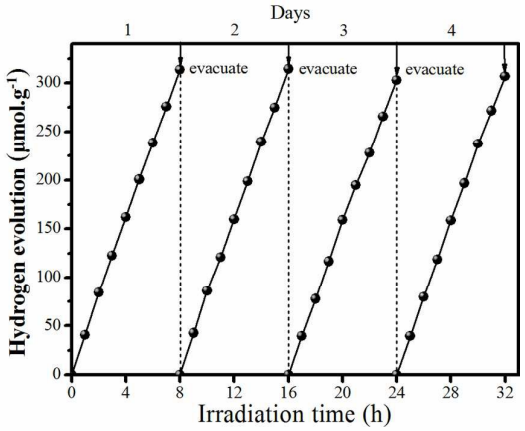

Fig.6 Recycling tests of hydrogen evolution over 3 wt% C,N-TiO_2 NPs/g-C_3N_4 nanocomposites under visible light irradiation.

Besides photocatalytic activity, the photo-stability is also an important parameter to estimate the catalysts for practical application. Therefore, recycling experiments of water splitting for H_2 generation were carried out at same photocatalytic condition. Fig. 6 shows the H_2 evolution curve of 3 wt% C,N-TiO_2 NPs/g-C_3N_4 photocatalyst in four consecutive days cycling photocatalytic runs. The results indicate that the photocatalytic performance of the composite presents no apparent deactivation with the exposure of irradiation for 32 h, indicating the excellent stability of C,N-TiO_2 NPs/g-C_3N_4 photocatalysts.

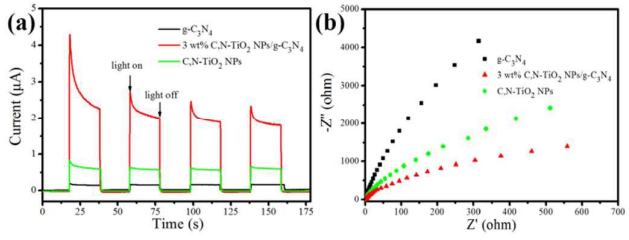

Fig.7 (a) Transient photocurrent responses and (b) electrochemical impedance spectroscopy (EIS) Nyquist plots of C,N-TiO_2 NPs, g-C_3N_4 and C,N-TiO_2 NPs/g-C_3N_4 nanocomposites in 0.1 M Na_2SO_4 solution.

It was well known that many factors, including the crystallinity, morphology, phase structure, light absorption, separation rate of photogenerated hole–electron pairs, play a key role in affecting the photocatalytic activity.[35,36] In the current work, the similarity of crystallinity, phase structure and microstructure should not be responsible for the remarkable enhancement of photocatalytic performance for H_2 production. The most important point deciding the photocatalytic activity may be the construction of close heterojunction interface, which dramatically faster the separation rate of charge carrier pairs. Conceivably, the importance of the heterogeneous interface in prompt charge migration was also illustrated in several previous reports.[37-41] To further prove this hypothesis, the faster separation rate of charge carrier pairs of C,N-TiO_2 NPs/g-C_3N_4 composites were characterized by photocurrent responses, EIS measurements and PL spectra. Fig.7a exhibits the photocurrent-time (I-t) curves of C,N-TiO_2 NPs, pure g-C_3N_4 as well as C,N-TiO_2 NPs/g-C_3N_4 hybrid material electrodes with several on-off cycles of intermittent irradiation. Obviously, the photocurrent obtained using 3 wt% C,N-TiO_2 NPs/g-C_3N_4 is significantly enhanced as comparison with the unitary component. As we known, the photocurrent is formed mainly by the diffusion of the photogenerated electrons to the back contact and meanwhile the photoinduced holes are taken by the hole acceptor in the electrolyte.[42] As a result, the enhanced photocurrent responses over the 3 wt% C,N-TiO_2 NPs/g-C_3N_4 hybrid composites reveals better charge separation and efficient electron transfer within the hybrid structure compared with those of bare C,N-TiO_2 NPs and pure g-C_3N_4. The more efficient transfer of charge carriers could be presented by the result of electrochemical impedance spectroscopy (EIS). The smaller frequency semicircle of the arc in an EIS Nyquist plot indicates the smaller resistance at the interface and the smaller charge-transfer resistance on the electrode surface. [43] The results of description in Fig.7b present the sequence of the frequency semicircles is: g-C_3N_4 > C,N-TiO_2 NPs > 3 wt% C,N-TiO_2 NPs/g-C_3N_4, which suggests the highest separation rate of charge carrier pairs over 3 wt% C,N-TiO_2 NPs/g-C_3N_4 photoanode, lowest over g-C_3N_4 photoanode. This also confirms that the construction of heterogeneous interface induces a more efficient separation of the photo-excited electron-hole pairs and lengthens the lifespan of the photo-generated charge carriers.

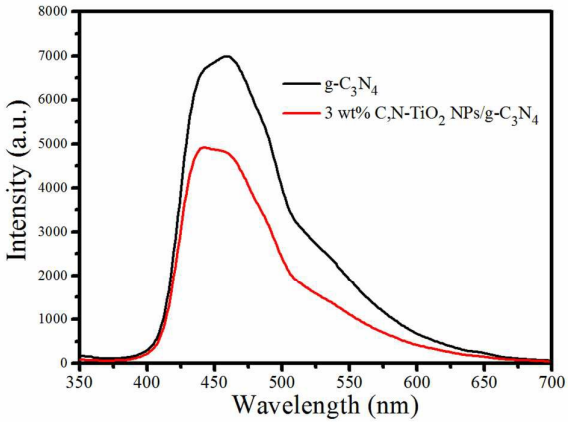

Fig.8 Room temperature PL spectra of g-C_3N_4 sample and 3 wt% C,N-TiO_2 NPs/g-C_3N_4 nanocomposites.

Photoluminescence (PL) spectroscopy originated from the recombination of photo-induced holes and electrons, the intensity of which could reflect the recombination rate of those free charge

carrier pairs.[44,45] Fig. 8 shows the fluorescence emission spectroscopy of pure g-C_3N_4 sample and 3 wt% C,N-TiO_2 NPs/g-C_3N_4 hybrid sample. It is clear that the fluorescence intensities of 3 wt% C,N-TiO_2 NPs/g-C_3N_4 is smaller than that of g-C_3N_4, signifying that the hybrid sample has lower recombination rate of the photoinduced electron-hole pairs than pure g-C_3N_4 sample. These results are in well agreement with the photocurrent test and EIS result, which further confirm it is the heterojunction interface that promotes the enhancement of separation rate of photo-generated hole-electron pairs, thereby significantly improving photocatalytic efficiency.

4. Conclusions

In conclusion, we present the design, fabrication and the related characterizations of C,N-TiO_2 NPs/g-C_3N_4 hybrid heterostructures for the photocatalytic H_2 evolution from water splitting. Compared to the bare C,N-TiO_2 NPs and pure g-C_3N_4 NSs, the sample of C,N-TiO_2 NPs/g-C_3N_4 composites exhibits much higher catalytic activity, especially 3 wt% C,N-TiO_2 NPs/g-C_3N_4 composite. Its H_2 generation rate is 10.9 folds and 21.3 folds than those of C,N-TiO_2 NPs and pure g-C_3N_4 NSs, respectively. The highly-efficient photocatalytic performance of the C,N-TiO_2 NPs/g-C_3N_4composite is attributed to improved light absorption and the close interfacial contact between the two components inducing the fast interfacial charge transfer from C,N-TiO_2 NPs to g-C_3N_4 nanosheets. Overall, this work provides a simple fabrication strategy yet promising prospect for the utilization of C,N-TiO_2 NPs/g-C_3N_4 as highly-efficient visible-light-driven photocatalyst for H_2 production without the presence of any noble metal co-catalyst.

Acknowledgements

This investigation was supported by the National Natural Science Foundation of China (Grant no. 51272107, 51372118 and 51572126) and the Fundamental Research Funds for the Central Universities (Grant no. 30920140132038).

Notes and references

1 A. Fujishima and K. Honda, *Nature*, 1972, **238**, 37-39.
2 A.G. Dosado, W.T. Chen, A. Chan, D. Sun-Waterhouse and G.I.N. Waterhouse, *J. Catal.*, 2015, **330**, 238-254.
3 D. Zheng, X. Pang, M. Wang, Y. He, C. Lin and Z. Lin, *Chem. Mater.*, 2015, **27**, 5271-5278.
4 Z.H.N. Al-Azri, W.T. Chen, A. Chan, V. Jovic, T. Ina, H. Idriss and G.I.N. Waterhouse, *J. Catal.*, 2015, **329**, 355-367.
5 L.L. Presti, M. Ceotto, F. Spadavecchia, G. Cappelletti, D. Meroni, R.G. Acres and S. Ardizzone, *J. Phys. Chem. C*, 2014, **118**, 4797-4807.
6 Q. Li, J. Bian, L. Zhang, R. Zhang, G. Wang and D.H.L. Ng, *ChemPlusChem*, 2014, **79**, 454-461.
7 B. Sambandam, A. Surenjan, L. Philip and T. Pradeep, *ACS Sustainable Chem. Eng.*, 2015, **3**, 1321-1329.
8 J.W.J. Hamilton, J.A. Byrne, P.S.M. Dunlop, D.D. Dionysiou, M. Pelaez, K. O' Shea, D. Synnott and S.C. Pillai, *J. Phys. Chem. C* 2014, **118**, 12206-12215.
9 H. Bai, K.S.Y. Kwan, Z. Liu, X. Song, S.S. Lee and D.D. Sun, *Appl. Catal. B*, 2013, **129**, 294-300.
10 Y. Li, J. Wang, Y. Yang, Y. Zhang, D. He, Q. An and G. Cao, *J. Hazard. Mater.*, 2015, **292**, 79-89.
11 J. Liu, H. Bai, Y. Wang, Z. Liu, X. Zhang and D.D. Sun, *Adv. Funct. Mater.*, 2010, **20**, 4175-4181.
12 R. Kaplan, B. Erjavec, G. Dražić, J. Grdadolnik and A. Pintar, *Appl. Catal. B*, 2016, **181**, 465-474.
13 Z. Hua, Z. Dai, X. Bai, Z. Ye, H. Gu and X. Huang, *J. Hazard. Mater.*, 2015, **293**, 112-121.
14 K. Sasan, F. Zuo, Y. Wang and P. Feng, *Nanoscale*, 2015, **7**, 13369-13372.
15 S.W. Shin, J.Y. Lee, K.S. Ahn, S.H. Kang and J.H. Kim, *J. Phys. Chem. C*, 2015, **119**, 13375-13383.
16 S. Cao and J. Yu, *J. Phys. Chem. Lett.*, 2014, **5**, 2101-2107.
17 J. Wang, J. Huang, H. Xie and A. Qu, *Int J Hydrogen Energy*, 2014, **39**, 6354-6366.
18 K. Li, S. Gao, Q. Wang, H. Xu, Z. Wang, B. Huang, Y. Dai and J. Lu, *ACS Appl. Mater. Interfaces*, 2015, **7**, 9023-9030.
19 J. Zhou, M. Zhang and Y. Zhu, *Phys. Chem. Chem. Phys.*, 2015, **17**, 3647-3652.
20 Q. Lin, L. Li, S. Liang, M. Liu, J. Bi and L. Wu, *Appl. Catal. B*, 2015, **163**, 135-142.
21 C. Han, Y. Wang, Y. Lei, B. Wang, N. Wu, Q. Shi and Q. Li, *Nano Res.*,2015,**8**, 1199-1209.
22 W. Chen, T.Y. Liu, T. Huang, X.H. Liu, J.W. Zhu, G.R. Duan and X.J. Yang, *Appl. Surf. Sci.*, 2015, **355**, 379-387.
23 H.J. Li, B.W. Sun, L. Sui, D.J. Qing and M. Chen, *Phys. Chem. Chem. Phys.*, 2015, **17**, 3309-3315.
24 W. Chen, T.Y. Liu, T. Huang, X.H. Liu, J.W. Zhu, G.R. Duan and X.J. Yang, J Mater. Sci., 2015, 50, 8142-8152.
25 K. Li, Z. Zeng, L. Yan, S. Luo, X. Luo, M. Huo and Y. Guo, *Appl. Catal. B*, 2015, **165**, 428-437.
26 M. Xiong, L. Chen, Q. Yuan, J. He, S.L. Luo, C.T. Au and S.F. Yin, *Carbon*, 2015, **86**, 217-224.
27 Y. He, L. Zhang, B. Teng and M. Fan, *Environ. Sci. Technol.*, 2015, **49**, 649-656.
28 Y. Yao, F. Lu, Y. Zhu, F. Wei, X. Liu, C. Lian and S. Wang, *J. Hazard. Mater.*, 2015, **297**, 224-233.
29 J. Sun, Y. Fu, G. He, X. Sun and X. Wang, *Appl. Catal. B*, 2015, **165**, 661-667.
30 W. Chen, G.R. Duan, T.Y. Liu, S.M. Chen and X.H. Liu, Mat. Sci. Semicond. Process. 35 (2015) 45-54.
31 K. Li, L. Yan, Z. Zeng, S. Luo, X. Luo, X. Liu, H. Guo and Y. Guo, *Appl. Catal. B*, 2014, **156-157**, 141-152.
32 H. Li, L. Zhou, L. Wang, Y. Liu, J. Lei and J. Zhang, *Phys. Chem. Chem. Phys.*, 2015, **17**, 17406-17412.
33 X. Li, P. Liu, Y. Mao, M. Xing and J. Zhang, *Appl. Catal. B*, 2015, **164**, 352-359.
34 Y. Cong, J. Zhang, F. Chen and M. Anpo, *J. Phys. Chem. C*, 2007, **111**, 6976-6982.
35 X. Bai, L. Wang and Y. Zhu, *ACS Catal.*, 2012, **2**, 2769 -2778.
36 Z. Luo, A.S. Poyraz, C.H. Kuo, R. Miao, Y. Meng, S.Y. Chen, T. Jiang, C. Wenos and S.L. Suib, *Chem. Mater.,* 2015, **27**, 6-17.
37 S. Meng, X. Ning, T. Zhang, S.F. Chen and X. Fu, *Phys. Chem. Chem. Phys.*, 2015, **17**, 11577-11585.
38 S. Chen, Y. Hu, S. Meng and X. Fu, *Appl. Catal. B*, 2014, **150-151**, 564-573.
39 J. Zhang, Y. Hu, X. Jiang, S. Chen, S. Meng and X. Fu, *J. Hazard. Mater.*, 2014, **280**, 713-722.
40 J. Di, J. Xia, S. Yin, H. Xu, L. Xu, Y. Xu, M. He and H. Li, *J. Mater. Chem. A*, 2014, **2**, 5340-5351.
41 M. Lu, Z. Pei, S. Weng, W. Feng, Z. Fang, Z. Zheng, M. Huang and P. Liu, *Phys. Chem. Chem. Phys.*, 2014, **16**, 21280-21288.
42 L. Yuan, M.Q. Yang and Y.J. Xu, *J. Mater. Chem. A*, 2014, **2**, 14401-14412.
43 J. Tong, L. Zhang, F. Li, M. Li, and S. Cao, *Phys. Chem. Chem. Phys.*, 2015, **17**, 23532-23537.

44 W. Chen, Z. Chen, T. Liu, Z. Jia and X. Liu, *J. Environ. Chem. Eng.*, 2014, **2**, 1889-1897.
45 S. Pany and K.M. Parida, *Phys. Chem. Chem. Phys.*, 2015, **17**, 8070-8077.

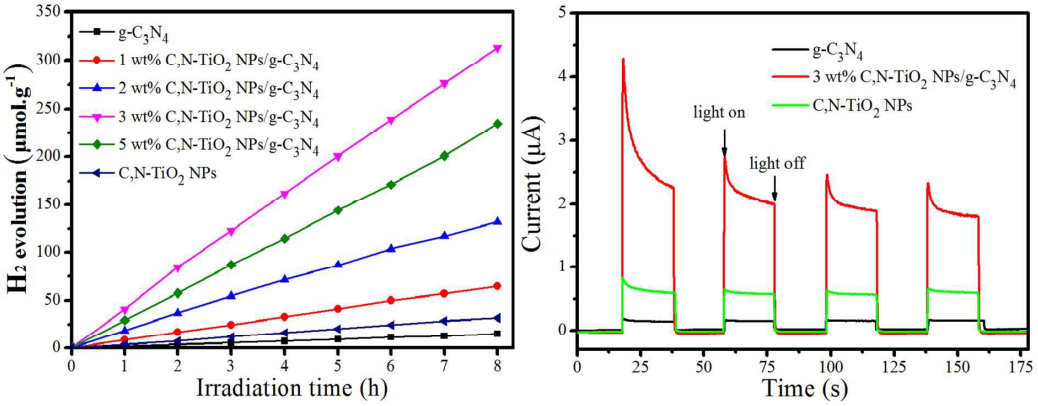

The improved visible photocatalytic H_2 evolution can be attributed to improved optical absorption and the lengthening lifetime of charge carriers' pairs as results of the C,N elmental codoping and the construction of intimate heterogeneous interface.